

Haze-level prior approach to enhance object visibility under atmospheric degradation

Vijaya Lakshmi THIRUMALA^{1*}, Venkata SatyaNarayana KARANAM²,
Pratap Reddy LANKIREDDY², Aruna Kumari KAKUMANI³, Rakesh Kumar YACHARAM⁴

¹Electronics and Communication Engineering, Mahatma Gandhi Institute of Technology, Hyderabad, India

²Electronics and Communication Engineering, Jawaharlal Nehru Technological University, Hyderabad, India

³Electronics and Communication Engineering, Vallurupalli Nageswara Rao Vignana Jyothi Institute of Engineering and Technology, Hyderabad, India

⁴Electronics and Communication Engineering, G. Narayanamma Institute of Technology and Science, Hyderabad, India

Received: 02.04.2020

Accepted/Published Online: 12.10.2020

Final Version: 30.03.2021

Abstract: Outdoor captured scenes are degraded by atmospheric particles and water droplets. Due to scattering and absorption effects in the atmosphere, degraded images lose contrast and color fidelity. Performances of the computer vision algorithms are bound to suffer from low-contrast scene radiance. In many single-image dehazing models, the larger the deviation in estimation of the key parameters such as transmission map and atmospheric light, the higher the halo artifacts and loss of fine details in the dehazed image. The available models assume that the scattering light is independent of wavelength, as the size of the atmospheric particles is larger compared to the wavelength of light. The model presented in this paper emphasizes the appropriate estimation of intensified transmission map from the hazy images by exploiting the scattering coefficient in order to address the issues of haze concentrations. Experiments conducted on thick and thin hazy images provide an optimal estimation of the model parameters, which can be applied directly in real-time situations. The available models are observed to be inconsistent sometimes in the enhancement of contrast, saturation and color information either together or independently. The proposed model addresses these issues by extracting the haze-relevant features from the hazy images, such as hue disparity, contrast, and darkness, which yield more vivid saturation results. Moreover, the proposed model addresses different haze densities in the scene without the use of refinement filters.

Key words: Dense haze, scattering coefficient of atmosphere, hue disparity, haze-level prior approach

1. Introduction

Most applications of computer vision deal with visualizing and interpreting real-time scenes. The issues prior to object detection are removal of background, spike points, and dead pixels. Outdoor/aerially captured images are significantly degraded due to particles suspended in the air like dust, water droplets, and aerosols [1]. Images captured at different climatic conditions exhibit poor visibility because of haziness [2–5], fog [6, 7], or blurriness in an image and require extra efforts for meaningful results. The severity of the weather conditions can be steady or dynamic depending on the size of the particles and their concentrations. The visibility range changes with the quantity and density of particles such as haze, fog, rainfall, and dust suspended in the air [8, 9]. The quantity and density of these particles are unpredictable as they vary with time and place. The higher the

*Correspondence: vijaya.chintala@gmail.com

density of the particles, the lower the visibility and the higher the attenuation. The presence of different sources of interference in imaging makes its modeling very challenging.

Haze in the atmosphere will degrade the outdoor captured images due to atmospheric absorption and scattering. Formation of haze is due to aerosol particles which produce a gray hue. The visual range of thin haze is between 4 and 10 km and that of dense haze is between 2 and 4 km. Fog is mainly formed by water droplets that produce a white hue. The visual range of thin fog varies from 1 to 2 km and that of dense fog varies up to 50 m. The attenuation due to the concentration of these floating particles have to be addressed effectively to improve the scene visibility.

The presence of environmental interferences makes the visibility of the image poor [10]. From low-level image analysis to high-level object recognition, a clear image is essential. The visibility of the scene can be improved by removing haze/fog as well as by correcting the color shifts caused by the air-light. Appearance modeling is composed of identifying visual object features for better representation of a region of interest and effective construction of mathematical models to detect objects [11, 12]. Degraded/low-visible images make object detection a more challenging computer vision problem with numerous real-world applications including human-computer interaction, autonomous vehicles, robotics, and surveillance and security systems [13–15]. In security systems, detecting suspicious objects like aerial/balloon bombs, airdropping of weapons, small explosive devices lying on the ground, and landmines, is a cumbersome task, when the scene radiance is degraded due to the atmospheric conditions.

Scattering of light by turbid medium is complicated and depends on the size, type, and orientation of the particles. This causes the outdoor images to have low contrast and color fidelity. The scattering phenomenon due to suspended particles leads to highly complex visual effects. The degraded image is spatially variant as the distance between the scene point and the camera depends on the amount of scattering. The scene intensity decreases exponentially with path length and the air-light increases with path length. Thus, the brightness of the scene point becomes apparent as the depth increases [16].

Scattering effects pose new challenges in the form of degradation on the computational aspects of image analysis [17]. Therefore, there is a need to model a framework for enhancement of images which is insensitive to environmental conditions. The key contribution of the proposed model is to conceptualize the essential features from hazy images to train a linear regression model in order to estimate the appropriate scattering coefficient for dehazing. The dehazing results obtained with the proposed work are far better compared to the available models for satellite- or drone-captured images. In this context, a few model-based restoration algorithms found from the literature are discussed as follows.

The model-based restoration algorithms are classified based on the number of input images needed for restoration. In multiimage haze models, images captured at different degrees of polarization using a polarizer [2, 4, 18] or a special imaging sensor [19, 20] were utilized for recovering the scenes' radiance. The performance of multiimage methods is better when compared to that of single-image methods, as they provide enough information for restoring the images. Perhaps, the need of special equipment for scene capturing attracted the researchers' attention to single-image dehazing.

Recently, significant efforts have been focused on single-image dehazing that relies on constrained priors and assumptions for scene recovery. Based on the characteristics and properties of hazy images, Tan et al. [21] worked on maximizing the local contrast for restoration. However, the results are not physically valid as it introduces blocking artifacts near the edges. The albedo or reflective power of the scene was estimated by Fattal et al. [22], based on the assumption that the surface shading and transmission medium are locally uncorrelated.

For instance, water albedo is about 10% of the incoming radiation whereas that of snow is 95%.

In a recent study, without considering any haze-related priors, the trainable systems were exploited in [23, 24] for dehazing. An end-to-end trainable system was proposed by Cai et al. [23]. The CNN proposed by Ren et al. [24] contains coarse-scale and fine-scale networks for predicting and refining the transmission map. These systems learn the mapping between hazy and transmission images with no priors. An integrated-prior-based deep-learning system was proposed in [25]. The proposed model is based on prior-based model and the overview of the prior-based algorithms is presented in the next section.

2. Overview of prior-based algorithms

The atmospheric degradation model was first introduced by McCartney in 1976 [26] and was further developed by Narasimhan [27, 28]. According to Narasimhan et al. [27, 28], the degradation due to atmospheric conditions is modeled by the key components viz. air-light and attenuation. The illumination reflected due to the source of light is defined as the air-light model. The light gets attenuated as it travels from the scene point and the viewer and is defined as the degradation model. Mathematically, the degradation model is depicted as follows:

$$I(p) = J(p)t(p) + A(1 - t(p)), \quad (1)$$

where $I(p)$ is low visible image due to atmospheric degradations, $J(p)$ is the actual scene, $t(p)$ is transmission medium, p the pixel index, and A represents air-light. The light reflected by the scenes' objects is attenuated before it reaches the camera. The emitted radiance from the object obviously decreases with the increase in the distance between the camera and the object [1, 16]. The first term in Equation 1 signifies that the intensities of the actual scene $J(p)$ gets attenuated with the distance and is given by

$$t(p) = e^{-\beta Z(p)}, \quad (2)$$

where β represents the scattering coefficient and $Z(p)$ represents the distance between the scene point and the camera. The second term in Equation 1 indicates that the brightness of the image increases, as the distance between the scene and the camera increases. The actual scene can be recovered arithmetically by

$$J'(p) = \frac{I(p) - A}{t(p)} + A. \quad (3)$$

Therefore, the ultimate goal of single-image dehazing is to estimate t and A with prior assumptions or knowledge, which is not trivial. Most of the earlier algorithms focus on estimating the atmospheric light, A [29], while several other studies focus on effectively estimating the transmission map, t [3, 30]. The popular prior-based algorithms for single-image dehazing are dark channel prior (DCP) proposed by He et al. [3] and color attenuation prior (CAP) proposed by Zhu et al. [30]. The inferences from these algorithms and their advancements are discussed as follows.

2.1. Dark channel prior

In DCP [3], the dark pixels in the RGB color channel of the image are found to estimate the haze transmission. The dark channel is basically the output of two minimum filters. To estimate the air-light component the most haze opaque region is identified by picking the top 0.1% of the brightest pixels in the dark channel. This approach is based on the assumption that at least one of the color channels in the image patches has pixels with

low intensities. However, this assumption is not valid when the objects in the scene are similar to air-light such as clouds, snow, white wall, and more of sky. The transmission map was estimated patch-wise, assuming that it is constant across a patch. This leads to severe halo effects at the edges.

Given a clear image $J(p)$, the hazy images are synthesized using the atmospheric scattering model described in Equations 1 and 2. The atmospheric light is assumed to be pure white and hence set to $[1,1,1]$ (RGB values). The synthetic images generated for different haze density levels (thick, moderate, and thin) with $t = 0.2, 0.5$ and 0.8 are shown in Figures 1b–1d, respectively, for the actual scene shown in Figure 1a. The recovery results obtained evaluating the DCP algorithm for thick, moderate, and thin haze densities are shown in Figure 1e. It greatly unveils the details of the images with shadows, colorful objects and dark surfaces or objects. Perhaps it introduces color distortions, changes the cloudy regions in the scene to yellow.

Meng et al. [31] extended the work on dark channel by regularizing the transmission around boundaries to mitigate its lack of resolution. The boundary constraint is combined with a weighted L1 norm regularization. Overall, it mitigates the lack of resolution in the DCP transmission map compared to that in He et al. [3], and the level of halo artifacts were reduced around sharp edges. However, these patch-wise strategies cannot deal with dense haze.

2.2. Color attenuation prior

In the CAP algorithm [30], the scene depth, $Z(p)$, of the hazy image was estimated by identifying color attenuation in the captured scene. The parameters of the linear model were derived by supervised training of the hazy images. The color attenuation of the objects in the scene was estimated by taking the difference between the brightness and saturation channels of the scene radiance in the CAP algorithm. Often, the white objects in the scene have high brightness and low saturation values, which makes the scene depth negligible. Estimating the atmospheric light and the depth information are the principle properties of transmission estimation. At moderate haze level the transmission error is less; however, the error is high at thin and thick haze density levels [16]. Accordingly, the visibility of the scene decreases.

The recovery results using this algorithm for thick, moderate, and thin haze densities are displayed in Figure 1f. The inferences from these results are: it performs well for moderate haze density levels; however, for thin and thick haze density levels, the results tend to either undersaturate or oversaturate. Hence, the model fails to address different haze density levels. Moreover, it also fails to recover nonhomogeneous hazy regions of an image, which is obvious in satellite- or drone-captured images.

As the size of the atmospheric particles is larger compared to the wavelength of light, in a myriad of restoration algorithms the scattering coefficient, β , is assumed to be constant [16, 30, 32]. This assumption suits only when the atmospheric model is homogeneous. Perhaps, in a real scenario, it is nonhomogeneous and considering the scattering coefficient to be constant or unity will not address different haze density levels.

The transmission medium is not only correlated with the scene depth, but also with the scattering coefficient as depicted in Equation 2. However, in the CAP algorithm [30] β is set to 1 and only depth map was considered to estimate the transmission map. To obtain an enhanced image, the properties of the medium have to be estimated. The visibility codes for different haze density levels [33] are shown in Table 1. It is notable from Table 1 that as the distance is increased, the scattering coefficient is decreased. In order to address different haze density levels, the scattering coefficient needs to be estimated. This work focuses on determining the scattering coefficient to address different haze density levels.

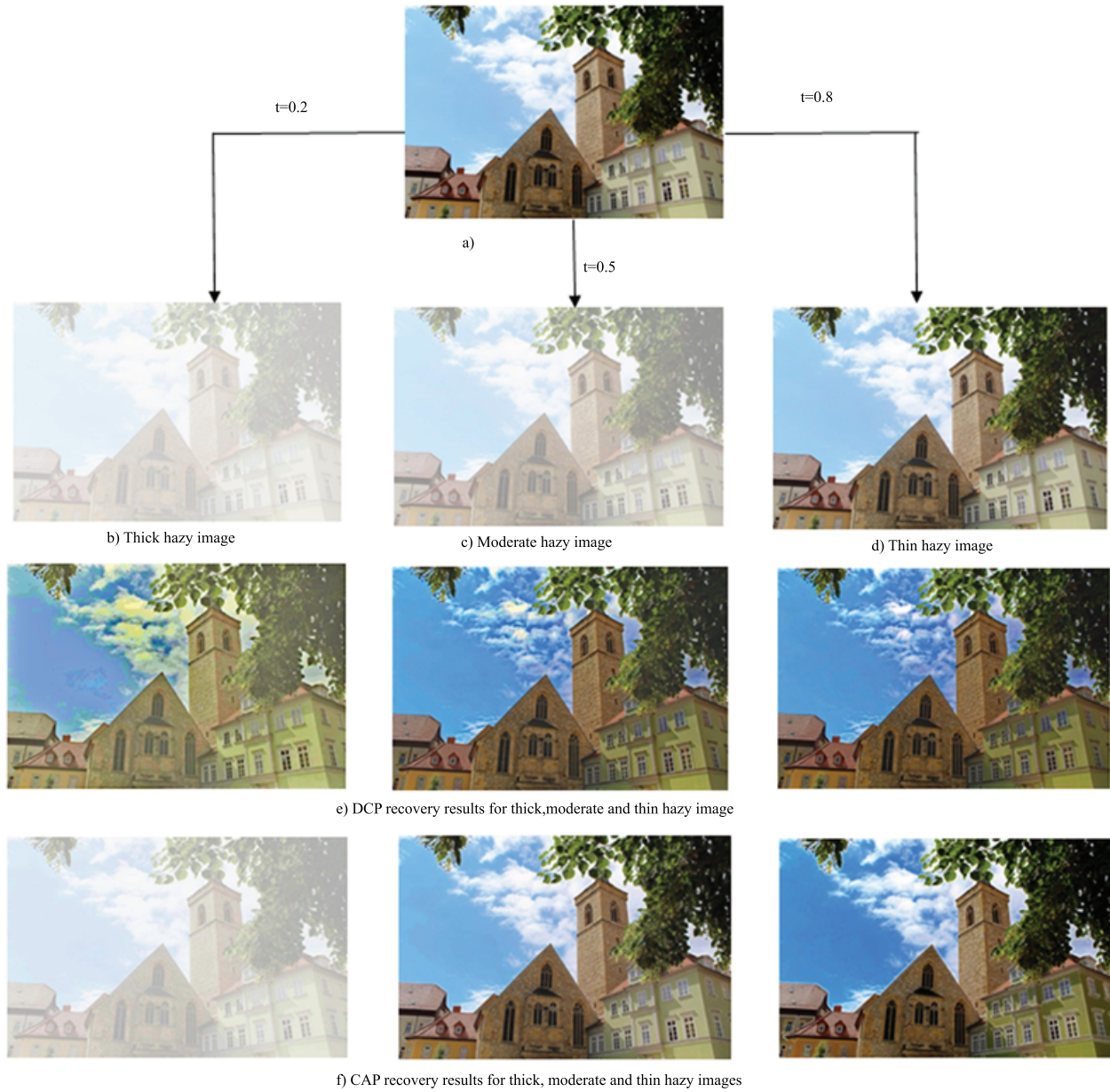


Figure 1. a)Actual scene, (b–d)synthetic hazy images obtained by changing t in Equation (1), (e–f) recovery results using the DCP and CAP algorithms.

2.3. Improved CAP models

In the advanced versions of CAP models [32, 34, 35], Gaussian [36, 37] and bilateral [38, 39] filters were used to refine the transmission map in order to sharpen the edges. To preserve the textures and edges in the color hazy images, cross-bilateral filter [40, 41], guided filter [42], and soft-matting [3] were employed [43–46]. Due to the similarity of spatial structures in the natural images, these strategies require redundant computations and transmission refining tools that lead to degrade the efficiency of haze removal. Although the abovementioned priors have advantages, they might result in vulnerable images and visual inconsistency.

Table 1. Visibility codes for haze density levels [33].

Haze level	Haze density	Metrological range (Z)	Scattering coefficient (β)
0	Clear	20–50 km	0.196–0.078
1	Thin haze	10–20 km	0.391–0.196
2	Moderate haze	4–10 km	0.954–0.391
3	Thick haze	2–4 km	1.96–0.954

In recent studies, several improvements on CAP model were found in the literature to address the limitations in CAP [47–50]. Zhang et al. [47] modeled the parameters of CAP nonlinearly and estimated the heterogeneous atmospheric light by employing the mean-pooling operation. The distribution of depth information was utilized to estimate the parameters through a supervised learning framework. However, it fails to estimate the correct depth maps for white objects. To address this, the depth map was refined with minimum and guided filters and then the filtered depth map was multiplied with a constant for further refinement. With such refined depth maps, their demonstrations conclude that the range of scattering coefficient, β , was bounded between [1.1, 2.0]. However, this interval of β cannot address images with different densities of haze as per the visibility codes specified in Table 1 [33].

Dat Ngo et al. [48] presented an improved version of CAP. At the preprocessing stage, the guided image filter used to refine the depth map in CAP [30] was replaced by a modified hybrid median filter. The atmospheric light was estimated using a quad-decomposition algorithm. The luminance channel was considered to overcome the unwanted influence of white objects. To avoid color distortion in the dark image regions after dehazing a weight factor was set in their algorithm. In addition to this, adaptive tone remapping was utilized to expand the dynamic range of the image at the postprocessing stage.

Kansal et al. [49] estimated the transmission map through subsampling mechanism and applying fast gradient domain guided filtering on CAP’s depth map. To compensate the nonuniform illumination variations in the CAP technique, Lambert’s law of illumination was proposed in [49]. In order to minimize the redundant computations, down-sampling is performed to preserve the local minimums in the resultant depth map. However, down-sampling may lead to loss of actual information (some times critical when we use satellite imagery).

Ju et al. [50] proposed the gamma correction prior (GCP) approach to overcome the limitations in gamma correction strategy [51]. The inverse image considered in [51] increases the contrast of the hazy image and thus poses serious drawbacks. To address the latent issues in the structure of the hazy images, the virtual image was considered in [50] to estimate the depth ratio information, and global optimization function was used for recovery. In this context, several factors were initialized manually in order to reduce the processing time needed for restoration. The correction factor (used to find the virtual image) was fixed to 0.5, although different values of this factor leads to different scattering coefficients. Moreover, down-sampling of the images is performed to estimate the stabilized scattering coefficient with minimal computations.

Although several remarkable improvements on CAP models were available in recent studies, the performance is still contingent. The existing strategies still suffer from adverse visual effects in the scene depth when the outdoor images are captured at different weather conditions and times of the day. This prompted us to design the haze-level prior model by estimating haze-relevant features from the hazy images to address different haze densities.

3. Haze-level prior model

The scattering coefficient, β , determines the intensity of dehazing [16]. Choosing a small value of β underestimates the transmission map and the objects in the scene still remains hazy in the distant regions. Large value of β overestimates the transmission and affects the fine details of the image [30]. Therefore, estimating the scattering coefficient is a daunting task which is addressed in the proposed model.

Evaluations are conducted on synthesized hazy images obtained from clear outdoor images having more of sky, water, snow, clouds, etc., captured during day and night. The synthetic images of different haze density levels (thick, moderate, and thin) are generated for clear images with $t = 0.2, 0.5$, and 0.8 , respectively. Sample mean square error (MSE) results obtained for different images using CAP algorithm [30] for different values of β are presented in Figure 2, for all three haze levels.

From the plots shown in Figure 2, it is notable that for thick hazy images the mean square error is minimum at $\beta = 1.75$, for moderate hazy images it is minimum at $\beta = 1$, whereas for thin hazy images it is minimum for $\beta \leq 0.5$. This clearly indicates that the concentrations of haze can be addressed by finding an appropriate value for β .

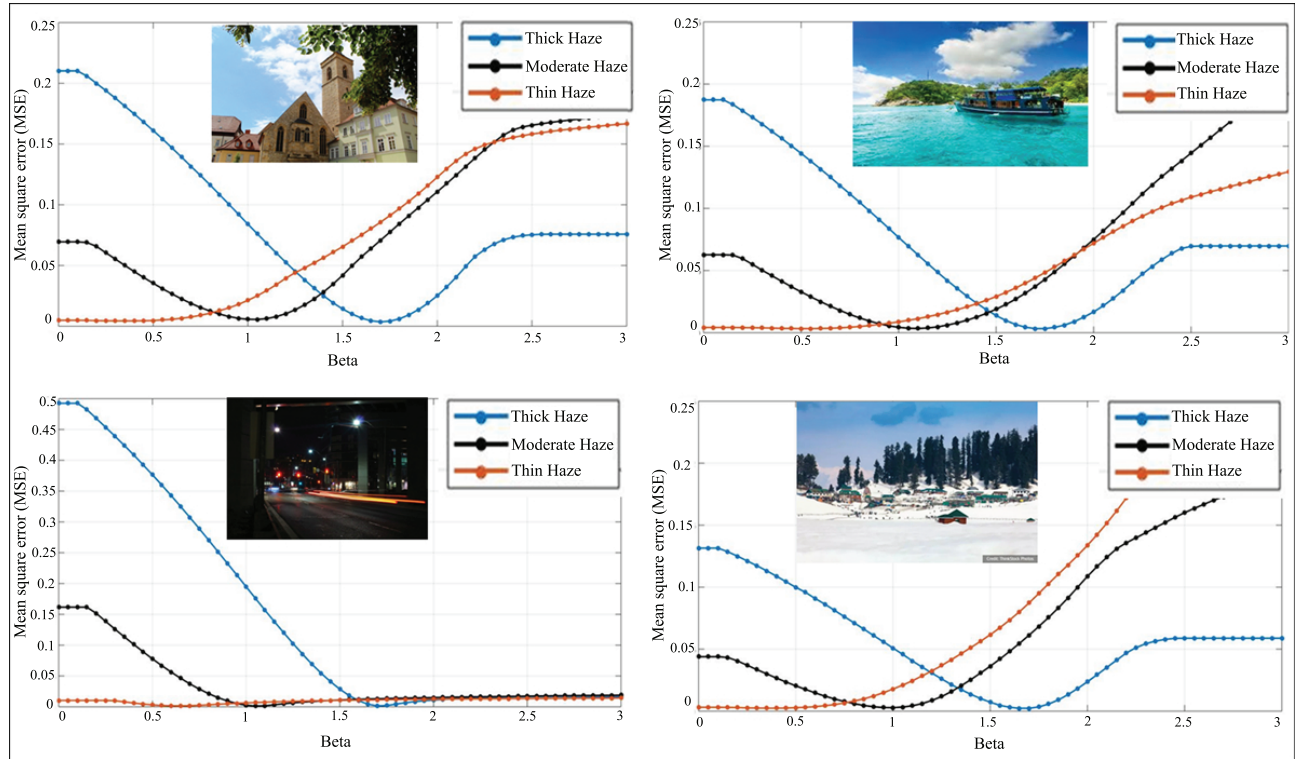


Figure 2. Mean Square errors obtained by synthesizing the corresponding outdoor images captured at different weather conditions and times of the day (along x-axis β is ranging from 0 to 3).

A few ideas from various earlier studies have been borrowed deliberately in the current work to adequately calculate the scattering coefficient. One such feature is hue disparity (HD) proposed in [52]. The authors in [52] proposed a semiinverse image and found its hue disparity with the original image. The semiinverse image, $I_{si}(p)$, is the maximum of $I^c(p)$ and $(1 - I^c(p))$ where c denotes the color channel. The difference between the

hue channels of original and semiinverse images is the hue disparity that can be used to estimate the haze level. The ‘semiinverse’ and ‘hue disparity’ results obtained for haze-free and hazy images are shown in Figures 3 and 4, respectively.

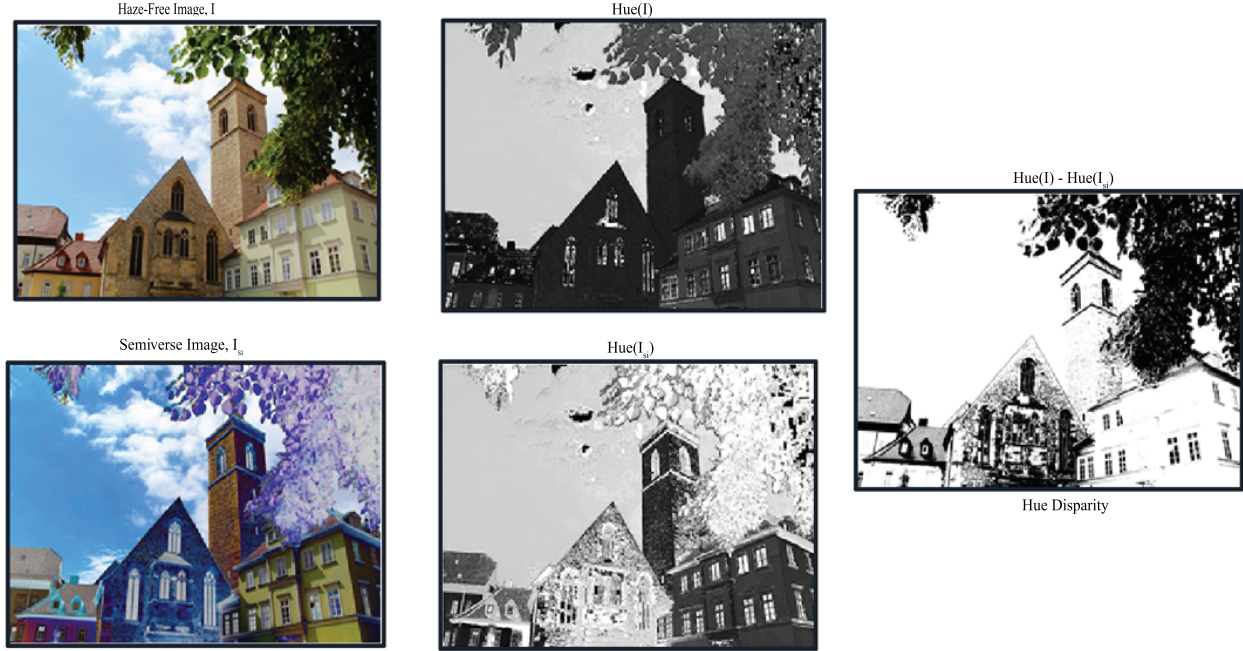


Figure 3. Semiinverse and hue disparity results for a haze-free image.

The semiinverse of a haze-free image differs from the original image (refer Figure 3), whereas that of a hazy image is similar to the original low-visible image (refer Figure 4). The hue disparity of haze-free and hazy images are different as barefaced from Figures 3 and 4, respectively. Hence, this feature helps to adequately differentiate the images captured at different haze density levels.

The pixels affected by haze will have high brightness and low saturation. Keeping this in view, the other two useful features considered in the current work are ‘contrast’ and ‘darkness’ of the given image to estimate the haze degree reliably and rapidly. Contrast is the difference between the bright, $b^I(p)$, and dark, $d^I(p)$, channels of the image, defined as follows.

$$b^I(p) = \max_{c \in \{r, g, b\}} I^c(p), \quad (4)$$

$$d^I(p) = \min_{c \in \{r, g, b\}} I^c(p). \quad (5)$$

In the current work the atmospheric light, A , and the scene depth, $Z(p)$, are computed using the algorithms developed in CAP [30]. The top 0.1% brightest pixels in $Z(p)$ were used to estimate A . The sample results of contrast (C), $A - d^I$, $A - HD$ for thin and thick hazy images are presented in Figure 5. For most of the thin hazy images, the average value of C is greater than 30 whereas that of $A - d^I$ and $A - HD$ are greater than 80. For most of the thick hazy images, the average values of C and $A - HD$ are less than 15 and

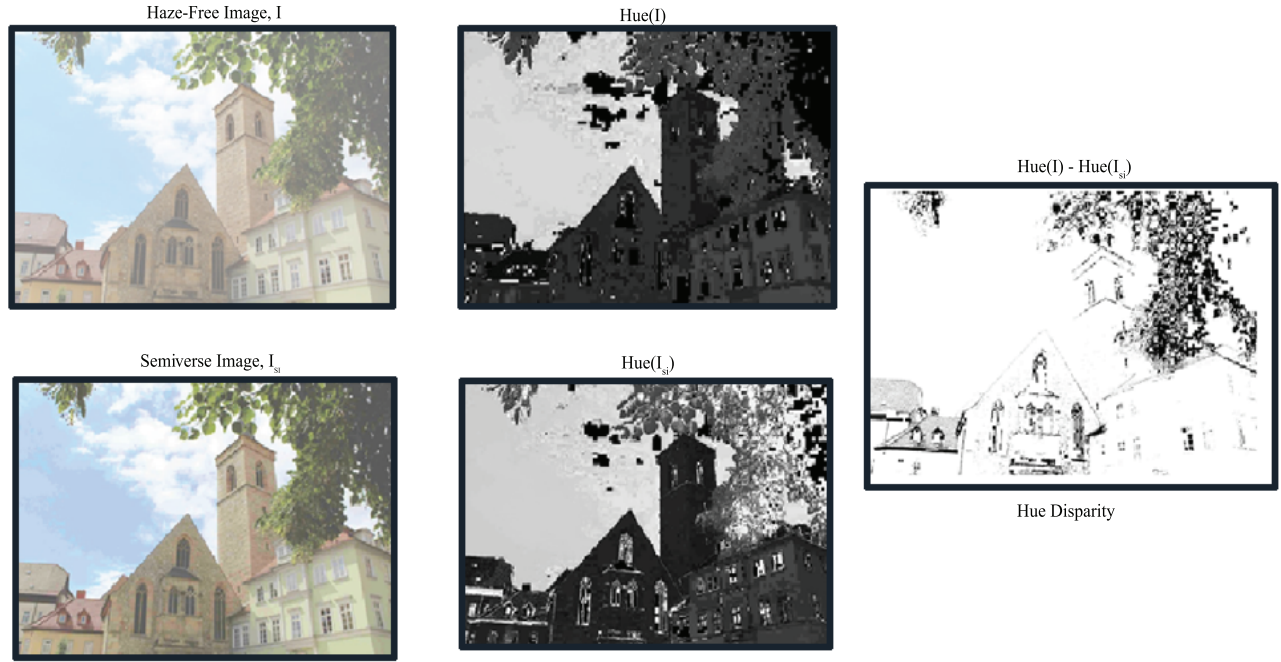


Figure 4. Semiinverse and hue disparity results for a hazy image.

that of $A - d^I$ is less than 50. The higher the values of C , $A - d^I$, and $A - HD$, the lower the value of β , and vice versa.

In order to estimate the haze level, the scattering coefficient, β , is formulated as depicted in Equation 6. Since β represents attenuation coefficient of the atmosphere, even atmospheric light, A , is also considered to significantly address the scenes having brighter air-light.

$$\beta = \frac{1}{a_1 x_1 + a_2 x_2 + a_3 x_3}, \quad (6)$$

where

$$x_1 = \frac{C}{A}; x_2 = \frac{A - d^I}{A}; x_3 = \frac{A - HD}{A}. \quad (7)$$

As $1/\beta$ is a linear function of x_1 , x_2 , x_3 variables, the relationship between these independent variables and the scattering coefficient is modeled with multiple linear regression, given 400 synthetic hazy images obtained with different t values. Based on the value of t used to generate the synthetic hazy image, its corresponding scattering coefficient from Table 1 is used to train the regression model to estimate its parameters. The experience constants a_1 , a_2 , and a_3 are statistically computed by multiple linear regression analysis on the synthetic data set $\langle \frac{1}{\beta_i}, x_{i1}, x_{i2}, x_{i3} \rangle$ for $i = 1$ to 400. The recommended values from the model $a_1 = 4$, $a_2 = 3$, and $a_3 = -1$ are used in the current work. More insights regarding the proposed model are described in Algorithm 1.






















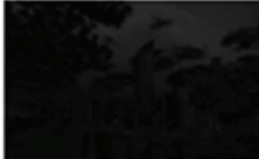


	Image	Contrast(C)	A - d ^I	A - HD	Average Values
Thin Haze					C = 53.23 A - d ^I = 151.84 A - HD = 94.67
					C = 36.5 A - d ^I = 212 A - HD = 182.5
					C = 60.4 A - d ^I = 154.5 A - HD = 107.5
Thick Haze					C = 10.1 A - d ^I = 30.2 A - HD = 3.4
					C = 7.2 A - d ^I = 42.5 A - HD = 15.6
					C = 11.9 A - d ^I = 30.8 A - HD = 14.3

Figure 5. Thin haze sample images with larger C , $A - d^I$, $A - HD$ and thick haze samples with smaller ones.

4. Results and discussions

Evaluations are conducted on 400 outdoor clear images collected from popular photo websites (e.g., Flickr, Google Images, and Picasaweb). Images captured at different atmospheric conditions and time of the day are considered for testing. In order to check the effectiveness of the haze-level prior model, synthetic hazy images are generated by varying t from 0.1 to 0.9 in Equation 1. Therefore, a total of 3600 (400×9) images are used

Algorithm 1 Haze-level prior modelInput: Actual scene $J(p)$, Natural Hazy image $I'(p)$ Output: Recovered Image $J'(p)$

Do the Job:

1. Generate synthetic hazy images $I(p)$ by varying t over the interval $[0.1 \ 0.9]$ in Equation 1
2. Estimate Depth map ($Z(p)$) and atmospheric light (A) of hazy images $I(p)$ using CAP [30].
3. Extract the following features from hazy image:
 - a. Find Semiinverse image, $I_{si}(p) = \max[I^c(p), (1-I^c(p))]$;
Compute Hue Disparity, $HD = I^H(p) - I_{si}^H(p)$, where H is the Hue channel of the image.
 - b. Find Contrast from bright and dark channels of the hazy image.
 $Contrast = b^I(p) - d^I(p)$
4. Train a linear regression model with the scattering coefficients described in Table 1 and the independent variables obtained from hazy images x_1 , x_2 , and x_3 (refer to Equation 7) to estimate the parameters a_1 , a_2 , and a_3 .
5. Given a natural hazy image $I'(p)$, Compute the Depth map and atmospheric light using CAP [30] and also compute the features described in step 3.
6. Estimate β using Equation 6, with the parameters estimated from step 4.
7. Estimate the transmission map, $t(p)$ using Equation 2.
8. Recover the dehazed image, $J'(p)$ using Equation 3.

in the evaluations (these images are different from the synthetic images used for training the multiple linear regression model).

The sample results obtained for synthetic thick ($t = 0.2$) and thin ($t = 0.8$) hazy images are compared with those of the proposed model in Figures 6 and 7. The actual scene and its zoom-in details of drone and satellite captured images are shown in Figures 6a–6b and 7a–7b, respectively. The synthetically generated hazy images are shown in Figures 6c and 7c. In order to improve the scene structure, the discontinuities in the depth information, i.e. the relative depth is measured in the proposed model by estimating the scattering coefficient. Hence, estimating the intensified transmission map from the hazy image leads to proper recovery. It is evident from the zoom-in details of the original image and the results (refer Figures 6 and 7) that different haze densities can be addressed by estimating the value of β unlike the CAP model (where β is set to 1).

Statistically, the performance of the proposed model is compared with those of the existing models in Table 2. The average MSE and SSIM results obtained for the synthetic hazy images are presented in Table 2. It is obvious from these results that the performance of the CAP and the proposed model are similar for moderate hazy images (i.e. for $t = 0.5$). This is because the scattering coefficient, β , is ‘1’ for moderate haze level. For other haze-levels, the performance of the proposed model is far better compared to that of the CAP model, as it estimates the haze-level prior to recovery. Statistically, the performance of the model developed in [48] exhibits its efficacy for moderate hazy images while the proposed model has proven its impact on thin and dense haze levels. The visual and the statistical performances of the proposed model are far better compared to those presented in [47].

The DCP algorithm introduces color shift, as the transmission medium is assumed to be constant in RGB color channels. Due to this, it turns the sky regions in the scene to yellow and cannot handle all types of weather conditions. The shortcomings of the DCP algorithm is that it cannot handle too bright objects and sunlight-influenced scenes and this is evident from the results shown in Figures 6d and 7d. In contrast, the proposed approach reduces the negative impact of bright objects or sky areas on the whole image.

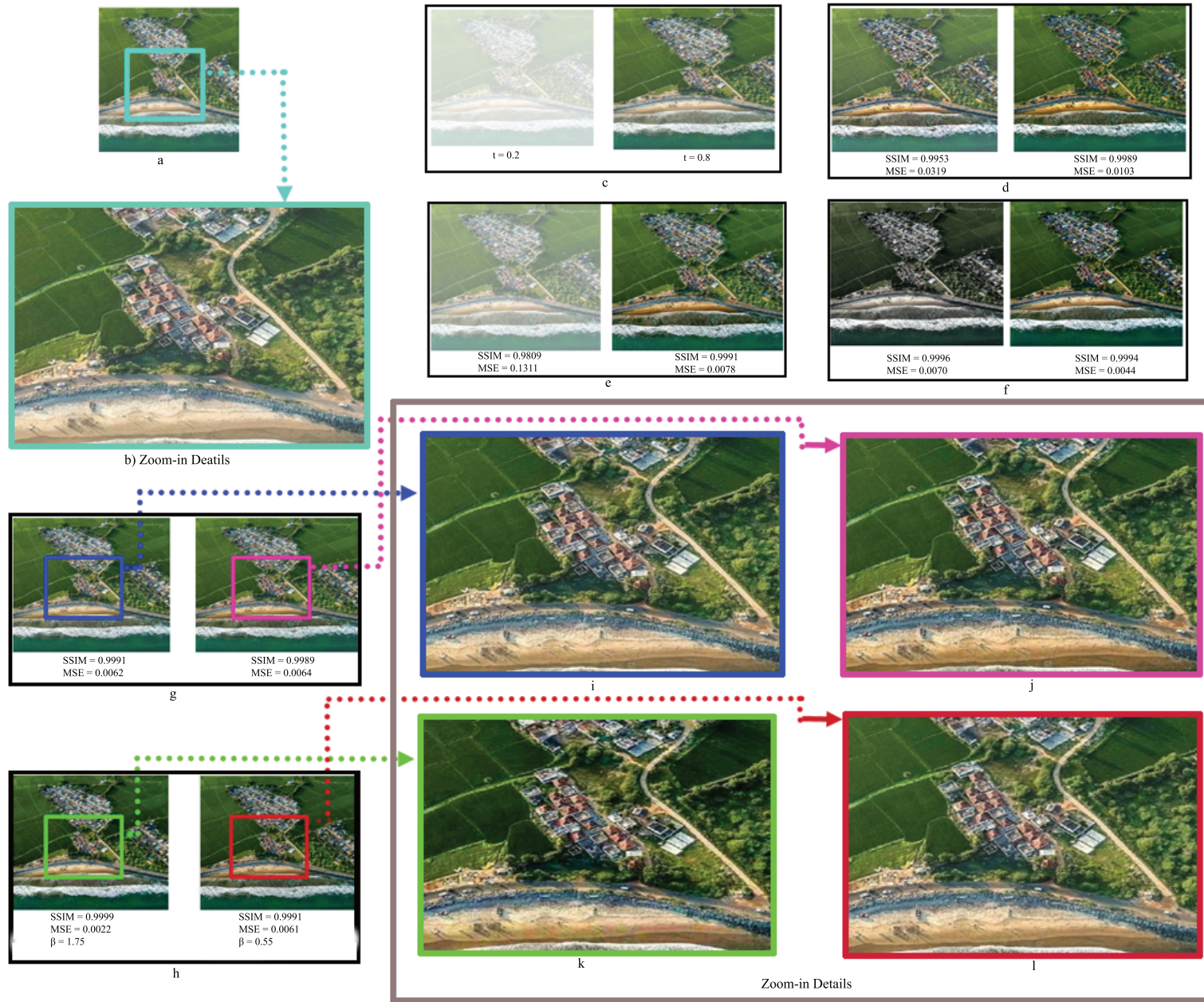


Figure 6. (a,b) Drone-captured scene and its zoom-in details, (c) synthetic hazy images, (d–h) recovery results for the synthetic hazy images shown in c, (d) DCP [3], (e) CAP [30], (f) nonlinear CAP [47], (g) improved CAP [48], (h) the proposed model, (i,j) zoom-in details of improved CAP, (k,l) zoom-in details of the proposed model.

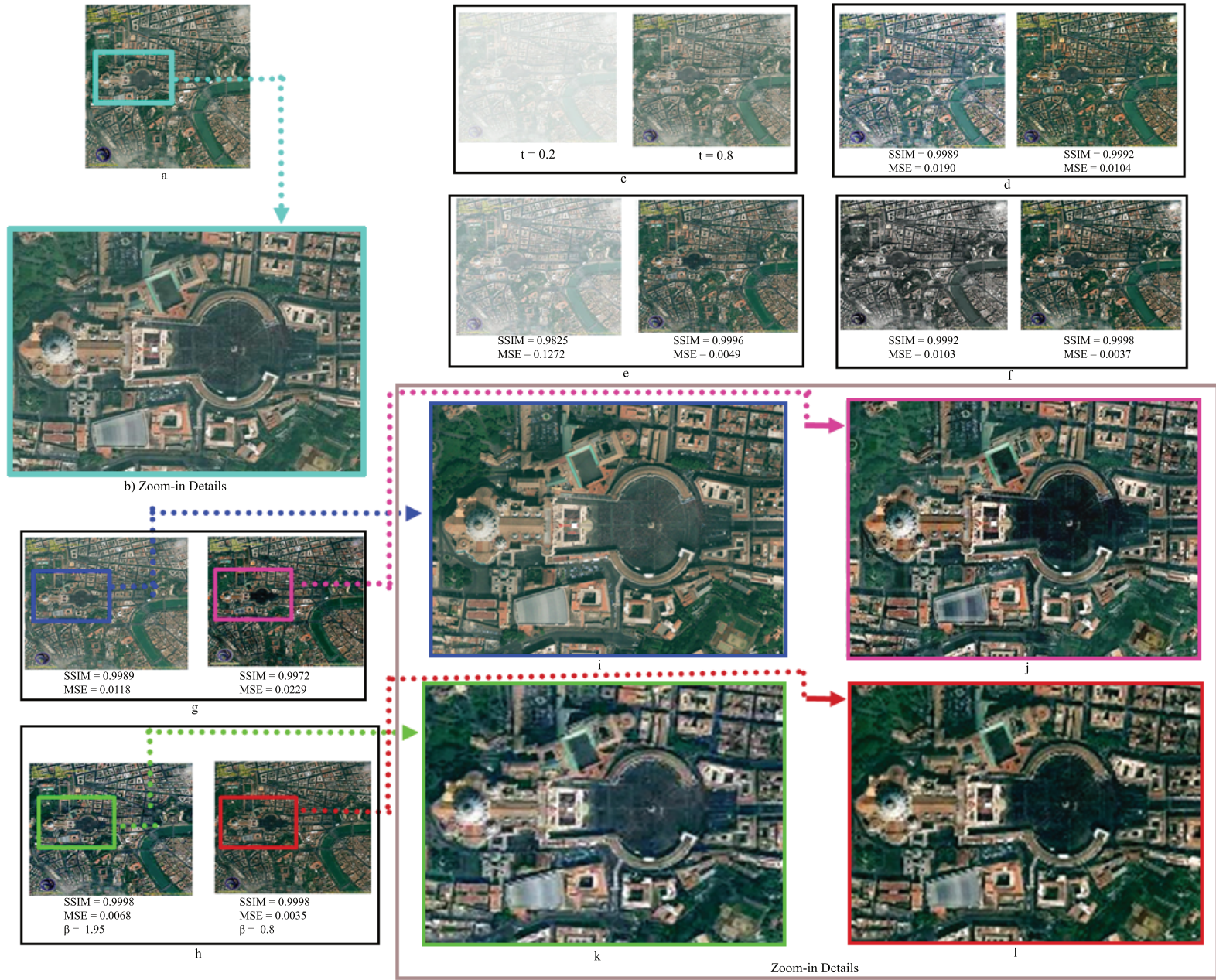


Figure 7. (a,b) Satellite captured scene and its zoom-in details, (c) synthetic hazy images, (d–h) recovery results for the synthetic hazy images shown in c, (d) DCP [3], (e) CAP [30], (f) nonlinear CAP [47], (g) improved CAP [48], (h) the proposed model, (i,j) zoom-in details of improved CAP, (k,l) zoom-in details of the proposed model.

CAP suffers from color distortion and loses the fine details in the scene (whether sky or nonsky regions) as depicted in Figures 6e and 7e. However, DCP performs well for nonsky regions in the scene, but it tends to darken the image while removing too much of haze. This is because in nonsky patches at least one of the color channels has pixels with low intensities, which makes room for dark channel. In contrast to this, estimating the haze-level prior preserves the detailed edges and realistic colors for both sky and nonsky regions of the scene. To make sure that the system preserves sharp edges and avoids halo artifacts while dehazing, intensified transmission maps are estimated in the current work.

Table 2. Comparison of the average results obtained for synthetic hazy images.

Synthetic hazy image with $t =$	CAP [30]		Nonlinear CAP [47]		Improved CAP [48]		Haze-level prior model		
	MSE	SSIM	MSE	SSIM	MSE	SSIM	MSE	SSIM	β
0.1	0.18	0.9785	0.2527	0.9707	0.0123	0.9991	0.0034	0.9999	2.35
0.2	0.084	0.99	0.1811	0.979	0.0079	0.9993	0.0036	0.9997	1.7
0.3	0.0337	0.9961	0.1274	0.9853	0.0058	0.9996	0.0041	0.9995	1.4
0.4	0.0115	0.9987	0.0867	0.9902	0.0047	0.9996	0.0053	0.9993	1.15
0.5	0.0057	0.99	0.0582	0.9935	0.0045	0.9995	0.0056	0.9991	1.05
0.6	0.0085	0.9983	0.0379	0.9958	0.0048	0.9994	0.005	0.9992	0.9
0.7	0.015	0.9966	0.0263	0.9968	0.0048	0.9993	0.0046	0.9994	0.75
0.8	0.0213	0.9948	0.0227	0.9966	0.0051	0.9992	0.0044	0.9995	0.35
0.9	0.0259	0.9931	0.0262	0.9966	0.0054	0.9991	0.0005	0.9997	0.05

The refined depth maps obtained in [47] limit the range of scattering coefficient over [1.1, 2.0]. However, this interval of β cannot address different haze concentrations according to the data specified in Table 1 [33]. From Figures 6f and 7f, it is also evident that the true colors of the image are not restored in case of dense hazy images. However, their visual and statistical performances of thin hazy images are closer with those of the proposed model.

Drone- and satellite-captured images are the point of interest for the present model and at the same time haze-level dependency of distance is another point of interest. Object and color information are crucial while analyzing images under haze distortions. Even though the difference in modeling is crucial, the evaluations also provide some amount of perception during subjective assessment. Keeping in view of the limitations, a brief comparison is provided. The dehazing results obtained with the improved CAP model [48] are shown in Figures 6g and 7g. The zoom-in details of these results are shown in Figures 6i, 6j, 7i, and 7j. The weight factor estimated in [48] to address color distortions has almost similar performance with reference to the proposed work. Although the performances of the improved CAP model [48] and the proposed model are statistically closer; visually, the jagged edges in satellite- or drone-captured images are more enhanced with the proposed work and the dehazing results obtained are displayed in Figures 6h and 7h with their zoomed versions in Figures 6k, 6l, 7k, and 7l. From the zoom-in detailed results of a drone-captured image shown in Figure 6k, it is evident that the thick hazy image is better addressed by the proposed model when compared to the other results. The performance of the improved CAP model is closer to the ground truth image.

To discuss the significance of the zoom-in details of satellite image with the improved CAP model (refer to Figure 7j), the edge details seem to be prominent when compared to the results obtained with the proposed model. However, the color distortions are quite visible at the center of the image when compared to its ground

truth. However, the hue disparity feature considered in the proposed model separates the intensity information from the principal color information which enhances the original colors of the scene without any loss or change of colors.

The estimated transmission maps obtained for the synthetic hazy images shown in Figures 6c and 7c are shown in Figures 8 and 9, respectively. For the synthetic hazy images shown in Figures 8a and 9a, the transmission maps obtained using CAP [30], nonlinear CAP [47], improved CAP [48], and the proposed model are depicted in Figures 8b–8e and 9b–9e, respectively.

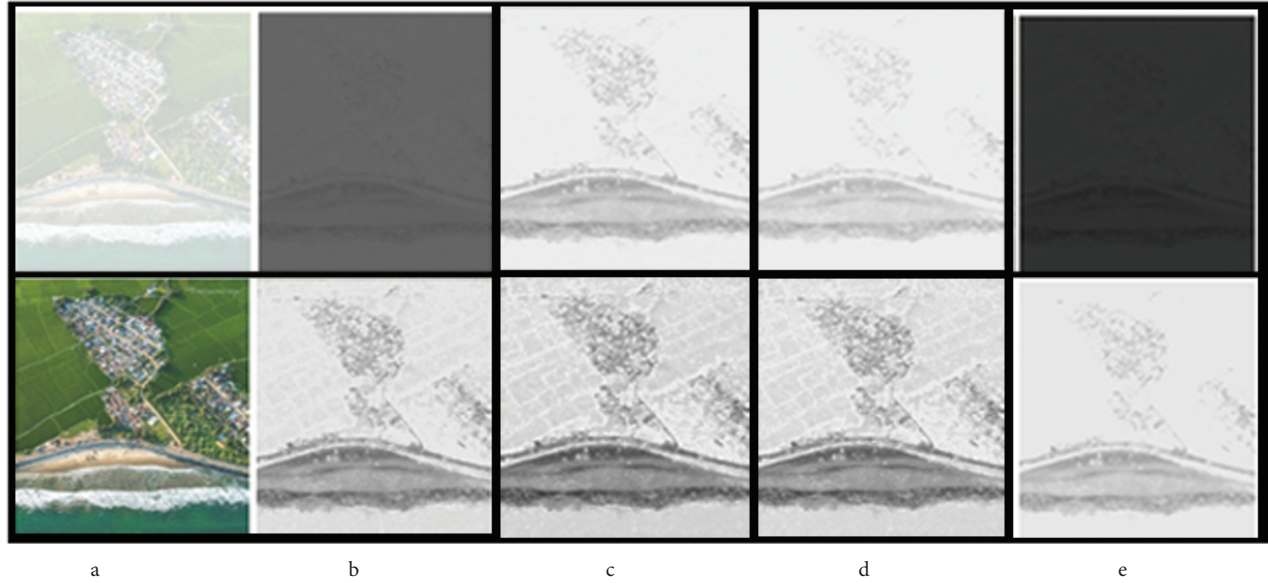


Figure 8. a) Synthetic hazy images shown in Figure 6c, (b–e) Estimated transmission maps, (b) CAP [30], (c) Nonlinear CAP [47], (d) improved CAP [48], (e) intensified transmission maps with the proposed model.

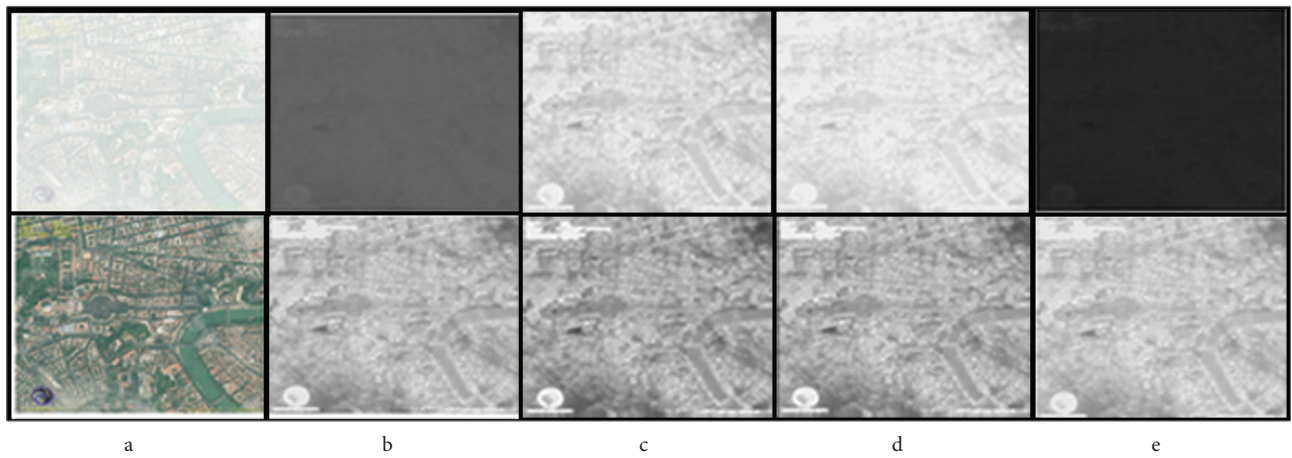


Figure 9. a) Synthetic hazy images shown in Figure 7c, (b–e) estimated transmission maps, (b) CAP [30], (c) nonlinear CAP [47], (d) improved CAP [48], (e) intensified transmission maps with the proposed model.

The recovery results obtained for real outdoor hazy images are compared with the existing models and are shown in Figure 10. For the real hazy images shown in Figure 10a, the dehazing results obtained using DCP [3], CAP [30], nonlinear CAP [47], improved CAP [48], and the proposed model are shown in Figures 10b–10f. The corresponding transmission maps obtained for real outdoor hazy images, shown in Figure 10a, using DCP [3], CAP [30], nonlinear CAP [47], improved CAP [48], and the proposed model are depicted in Figures 11a–11e. As all the priors do not hold true in all circumstances, even the proposed prior has a pitfall. The limitation observed with the proposed model is that it tends to amplify the halo effects of the images having rain reflections of headlights of a vehicle.

The idea of the GCP model [50] is to mine the depth structure information from virtual hazy image obtained by fixing the gamma correction factor. At the same time, estimation of scattering coefficient is carried out on down-sampled images. The GCP [50] and improved CAP [49] models attempted to down-sample the images, resulting in possible loss of information with respect to satellite images.

The proposed model attempted to retain the entire information pertaining to the original image without any kind of down-sampling. This fundamental difference between the models will make a huge difference in the application areas which will conceptually alter the expected outcome as well as concrete details of the scene or objects in a real scenario. The visualization of image structures and contrast in heavy-haze regions can be improved with the proposed model, while restoring the faithful colors. It also augments the structures such as jagged edges, corners, and exhibit its efficacy in recovering satellite- and drone-captured images.

5. Conclusion

Numerous applications of computer vision deal with visualization and interpretation of real-time scenes which often get degraded due to atmospheric interference. Aerially captured images are significantly degraded due to suspended atmospheric particles. The quantity and density of these particles are unpredictable as they keep varying with time and space. A clear image is highly essential in image analysis and object recognition phases. Inaccurate estimation of a transmission map introduces severe distortions. In order to estimate the transmission medium accurately, an appropriate or closely accurate estimate of relative scene depth is expected. The scattering coefficient, which determines the intensity of dehazing, is exploited in the current work by estimating the intensified transmission map from dehazed images. The proposed haze-level prior model has performed well for dense haze levels. The negative impact due to bright objects or sky areas on the whole image is also reduced. In the future, this model can be extended to address nonhomogeneous hazy scenes by estimating the scattering coefficient patch-wise from a hazy image. The air-light is assumed to be pure-white, which may not address the color offset of haze particles and light sources. Due to this, the limitation observed with the proposed model is that it tends to amplify the halo effects of the images having rain reflections of headlights of a vehicle. As part of future work, we intend to extend our work to address this issue by considering different values of air-light.

Acknowledgments

This work is funded by TEQIP-III, JNTU, Hyderabad, India with Proc. No. JNTUH/TEQIP-III/CRS/2019/ECE/04. The authors gratefully acknowledge the funding agency for their extended support. A special thanks to Ms.K.Lakshmi Bhavani for her constant and timely support throughout the project. We also thank the editor and the reviewers for their constructive comments and suggestions to improve the quality of the manuscript.



Figure 10. a) Natural outdoor hazy scenes, (b–f) recovery results obtained using (b) DCP [3], (c) CAP [30], (d) nonlinear CAP [47], (e) improved CAP [48], and (f) the proposed model.



Figure 11. Estimated transmission maps for natural outdoor scenes shown in Figure 10 (a) DCP [3], (b) CAP [30], (c) nonlinear CAP [47], (d) improved CAP [48], and (e) the proposed model.

References

- [1] Liang D, Kaneko S, Hashimoto M, Iwata K, Zhao X et al. Robust object detection in severe imaging conditions using co-occurrence background model. *International Journal of Optomechatronics* 2014; 8 (1): 1559-9612. doi: 10.1080/15599612.2014.890686
- [2] Liang J, Ren L, Ju H, Zhang W, Qu E. Polarimetric dehazing method for dense haze removal based on distribution analysis of angle of polarization. *Optics Express* 2015; 23 (9): 26146. doi: 10.1364/OE.23.026146

- [3] He K, Sun J, Tang X. Single image haze removal using dark channel prior. *IEEE Transactions on Pattern Analysis and Machine Intelligence* 2011; 33 (12): 2341-2353. doi: 10.1109/TPAMI.2010.168
- [4] Fang S, Xia X, Huo X, Chen C. Image dehazing using polarization effects of objects and airlight. *Optics Express* 2014; 22 (16). doi: 10.1364/OE.22.019523
- [5] Lu H, Li Y, Zhang L, Serikawa S. Contrast enhancement for images in turbid water. *Journal of the Optical Society of America* 2015; 32 (5): 886-93. doi: 10.1364/JOSAA.32.000886
- [6] Zhu Y, Tang G, Zhang X, Jiang J, Tian Q. Haze removal method for natural restoration of images with sky. *Neurocomputing* 2017; 275 (9): 499-510. doi: 10.1016/j.neucom.2017.08.055
- [7] Farhan H, Jechang J. Visibility enhancement of scene images degraded by foggy weather conditions with deep neural networks. *Journal of Sensors* 2016; (2016): 3894832:1-3894832:9. doi: 10.1155/2016/3894832
- [8] Alkholidi A. Free space optical communications — theory and practices. In: Mutamed Khatib (editor). *Wireless Communications*. 1st ed. INTECH 2014, pp. 159-212. doi: 10.5772/58884
- [9] Makarau A, Richter R, Müller R, Reinartz P. Haze detection and removal in remotely sensed multispectral imagery. *IEEE Transactions on Geoscience and Remote Sensing* 2014; 52: 5895-5905. doi: 10.1109/TGRS.2013.2293662
- [10] Rasti B, Scheunders P, Ghamisi P, Licciardi G, Chanussot J. Noise reduction in hyperspectral imagery: Overview and application. *Remote Sensing* 2018; 10 (3) 482-510. doi: 10.3390/rs10030482
- [11] Chen Z, Li X, Zheng H, Gao H, Wang H. Domain adaptation and adaptive information fusion for object detection on foggy days. *Sensors* 2018; 18 (10) 3286. doi: 10.3390/s18103286
- [12] Liu X, Hardeberg JY. Fog removal algorithms: Survey and perceptual evaluation. In: *IEEE 2013 European Workshop on Visual Information Processing*; Paris, France; 2013. pp. 118-123.
- [13] Lu Y, xiang Huang Q. Object detection algorithm in underground mine based on sparse representation. *International Journal of Advancements in Technology* 2018; 9 (1). doi: 10.4172/0976-4860.1000210
- [14] Fiaz M, Mahmood A, Soon Ki Jung. Tracking noisy targets: A review of recent object tracking approaches. *ArXiv abs/1802.03098* (2018).
- [15] Kowalski M, Kastek M, Palka N, Polakowski H, Szustakowski M et al. Investigations of concealed objects detection in visible, infrared and terahertz ranges. *PHOTONICS LETTERS OF POLAND* 2018; 5 (4) 167-169. doi: 10.4302/plp.2013.4.16
- [16] Narasimhan S, Nayar S. Vision and the atmosphere. *International Journal of Computer Vision* 2002; 48 (3) 233-254. doi: 10.1145/1508044.1508113
- [17] Chavez PS. An improved dark-object subtraction technique for atmospheric scattering correction of multispectral data. *Remote Sensing of Environment* 1998; 24 (3) 459-479. doi: 10.1016/0034-4257(88)90019-3
- [18] Liang J, Ren L, Ju H, Qu E, Wang Y. Visibility enhancement of hazy images based on a universal polarimetric imaging method. *Journal of Applied Physics* 2014; 116 (17) 173107. doi: 10.1063/1.4901244
- [19] Kermani E, Asemani D. A robust adaptive algorithm of moving object detection for video surveillance. *EURASIP Journal on Image and Video Processing* 2014; 2014 (1):27. doi: 10.1186/1687-5281-2014-27
- [20] Ozaki M, Kakimura K, Hashimoto M, Takahashi K. Laser-based pedestrian tracking in outdoor environments by multiple mobile robots. *Sensors* 2012; 12 (11) 14489-507. doi: 10.3390/s121114489
- [21] Tan R. Visibility in bad weather from a single image. In: *IEEE 2008 Conference on Computer Vision and Pattern Recognition*; Anchorage, AK, USA; 2008. pp. 1-8.
- [22] Fattal R. Single image dehazing. *ACM Transactions on Graphics* 2008; 27 (3) 1-9. doi: 10.1145/1399504.1360671
- [23] Cai B, Xu X, Jia K, Qing C, Tao D. Dehazenet: An end-to-end system for single image haze removal. *IEEE Transactions on Image Processing*; 2016, 25(11) 5187-5198. doi: 10.1109/TIP.2016.2598681

- [24] Ren W, Liu S, Zhang H, Pan J, Cao X et al. Single image dehazing via multi-scale convolutional neural networks. *Computer Vision – ECCV 2016*; Cham, Switzerland: Springer International Publishing, 2016, pp. 154-169.
- [25] Yang D, Sun J. Proximal dehaze-net: A prior learning-based deep network for single image dehazing. *Computer Vision – ECCV 2018*; Cham: Springer International Publishing, 2018, pp. 729-746.
- [26] Cantor A. Optics of the atmosphere–scattering by molecules and particles. *IEEE Journal of Quantum Electronics* 1978; 14 (9) 698-699. doi: 10.1109/JQE.1978.1069864
- [27] Nayar SK, Narasimhan SG. Vision in bad weather. In: *Proceedings of the Seventh IEEE International Conference on Computer Vision*; Kerkyra, Greece, Greece; 1999 pp. 820-827.
- [28] Narasimhan SG, Nayar SK. Contrast restoration of weather degraded images. *IEEE Transactions on Pattern Analysis and Machine Intelligence* 2003; 25 (6) 713-724. doi: 10.1109/TPAMI.2003.1201821
- [29] Sulami M, Glatzer I, Fattal R, Werman M. Automatic recovery of the atmospheric light in hazy images. In: *IEEE 2014 International Conference on Computational Photography*; Santa Clara, CA, USA; 2014 pp. 1-11.
- [30] Zhu Q, Mai J, Shao L. A fast single image haze removal algorithm using color attenuation prior. *IEEE Transactions on Image Processing* 2015; 24 (11) 3522-3533. doi: 10.1109/TIP.2015.2446191
- [31] Meng G, Wang Y, Duan J, Xiang S, Pan C. Efficient image dehazing with boundary constraint and contextual regularization. In: *2013 IEEE International Conference on Computer Vision*; Sydney, NSW, Australia; 2013 pp. 617-624.
- [32] Jeong S, Lee S. The single image dehazing based on efficient transmission estimation. In: *IEEE 2013 International Conference on Consumer Electronics*; Las Vegas, NV, USA; 2013 pp. 376-377.
- [33] Hulburt EO. Optics of atmospheric haze. *Journal of the Optical Society of America* 1941; 31 (7) 467-476. doi: 10.1364/JOSA.31.000467
- [34] Huang S, Chen B, Wang W. Visibility restoration of single hazy images captured in real-world weather conditions. *IEEE Transactions on Circuits and Systems for Video Technology* 2014; 24 (10) 1814-1824. doi: 10.1109/TCSVT.2014.2317854
- [35] Cheng Y, Chen B, Huang S, Kuo S, Kopylov A. Visibility enhancement of single hazy images using hybrid dark channel prior. In: *IEEE 2013 International Conference on Systems, Man, and Cybernetics*; Manchester, UK; 2013 pp. 3627-3632.
- [36] Yang H, Wang J. Color image contrast enhancement by co-occurrence histogram equalization and dark channel prior. In: *Proceedings - 2010 3rd International Congress on Image and Signal Processing*; Yantai, China; 2010 pp. 659-663.
- [37] Long J, Shi Z, Tang W. Fast haze removal for a single remote sensing image using dark channel prior. In: *2012 International Conference on Computer Vision in Remote Sensing*; Xiamen, China; 2012 pp. 132-135.
- [38] Xu H, Guo J, Liu Q, Ye L. Fast image dehazing using improved dark channel prior. In: *Proceedings of International Conference on Information Science and Technology*; Hubei, China; 2012 pp. 663-667. doi: 10.1109/ICIST.2012.6221729
- [39] Yu J, Xiao C, Li D. Physics-based fast single image fog removal. In: *IEEE 2010 International Conference on Signal Processing Proceedings*; Beijing, China; 2010, pp. 1048-1052.
- [40] Xiao C, Gan J. Fast image dehazing using guided joint bilateral filter. *The Visual Computer* 2012; 28 (6) 713-721. doi: 10.1007/s00371-012-0679-y
- [41] Lv X, Chen W, Shen I. Real-time dehazing for image and video. In: *2010 18th Pacific Conference on Computer Graphics and Applications*; NW Washington, DC, United States; 2010, pp. 62-69.
- [42] Linan Y, Yan P, Xiaoyuan Y. Video defogging based on adaptive tolerance. *TELKOMNIKA Indonesian Journal of Electrical Engineering* 2012; 10 (7) 1644-1654. doi: 10.11591/telkomnika.v10i7.155

- [43] Zhang Y, Ding Y, Xiao J, Liu J, Guo Z. Visibility enhancement using an image filtering approach. *EURASIP Journal on Advances in Signal Processing* 2012; 2012 (220) pp. 1-6, 10. doi: 10.1186/1687-6180-2012-220
- [44] Lan X, Zhang L, Shen H, Yuan Q, Li H. Single image haze removal considering sensor blur and noise. *EURASIP Journal on Advances in Signal Processing* 2013; 86. doi: 10.1186/1687-6180-2013-86
- [45] Wang JB, He N, Zhang LL, Lu K. Single image dehazing with a physical model and dark channel prior. *Neurocomputing* 2015; 149 (B) 718-728. doi: 10.1016/j.neucom.2014.08.005
- [46] Kil T, Lee S, Cho N. Single image dehazing based on reliability map of dark channel prior. In: *IEEE 2013 International Conference on Image Processing*; Melbourne, VIC, Australia; 2013 pp. 882-885. doi: 10.1109/ICIP.2013.6738182
- [47] Zhang S, Qing C, Xu X, Jin J, Qin H. Dehazing with improved heterogeneous atmosphere light estimation and a nonlinear color attenuation prior model. In: *2016 10th International Symposium on Communication Systems, Networks and Digital Signal Processing (CSNDSP)*, Prague, Czech Republic; 2016, pp. 1-6. doi: 10.1109/CSNDSP.2016.7573967
- [48] Ngo D, Lee GD, Kang B. Improved color attenuation prior for single-image haze removal. *Applied Sciences* 2019; 9 (19) 4011. doi: 10.3390/app9194011
- [49] Kansal I, Kasana SS. Improved color attenuation prior based image de-fogging technique. *Multimedia Tools and Applications*; 2020, 01. doi: 10.1007/s11042-019-08240-6
- [50] Ju M, Ding C, Guo YJ, Zhang D. Idgcp: Image dehazing based on gamma correction prior. *IEEE Transactions on Image Processing* 2020, 29 3104-3118. doi: 10.1109/TIP.2019.2957852
- [51] Liu C, Zhao J, Shen Y, Zhou Y, Wang X et al. Texture filtering based physically plausible image dehazing. *The Visual Computer* 2016, 32 (6-8). doi: 10.1007/s00371-016-1259-3
- [52] Ancuti CO, Ancuti C, Hermans C, Bekaert P. A fast semi-inverse approach to detect and remove the haze from a single image. In: *ACCV 2010 - 10th Asian Conference on Computer Vision*; Queenstown, New Zealand; 2011. pp. 501-514.